Geochemistry 79 (2019) 125518

Contents lists available at ScienceDirect

Geochemistry

journal homepage: www.elsevier.com/locate/chemer

A light, chondritic xenolith in the Murchison (CM) chondrite – Formation by fluid-assisted percolation during metasomatism?

Imene Kerraouch[a,*], Samuel Ebert[b], Markus Patzek[b], Addi Bischoff[b], Michael E. Zolensky[c], Andreas Pack[d], Philippe Schmitt-Kopplin[e,f], Djelloul Belhai[a], Abderrahmane Bendaoud[a], Loan Le[g]

[a] LGGIP, FSTGAT, Université des Sciences et de la Technologie Houari Boumediene, Alger, Algeria
[b] Institut für Planetologie, Westfälische Wilhelms-Universität Münster, Wilhelm-Klemm Str. 10, D-48149 Münster, Germany
[c] ARES, NASA Johnson Space Center, Houston, TX, USA
[d] Universität Göttingen, Geowissenschaftliches Zentrum, Goldschmidtstr. 1, D-37077 Göttingen, Germany
[e] Helmholtz-Zentrum, München, German Research Center for Environmental Health, Analytical BioGeoChemistry, Ingolstädter Landstraße 1, D-85764 Neuherberg, Germany
[f] Chair of Analytical Food Chemistry, Technische Universität München, D-85354 Freising-Weihenstephan, Germany
[g] Jacobs ESCG, Houston, TX 77058, USA

ARTICLE INFO

Handling Editor: Falko Langenhorst

Keywords:
Murchison
White clast
Carbonaceous chondrite
Metamorphism
Percolation
Brecciation

ABSTRACT

The main mineralogical characteristics of a large light-colored clast within the Murchison CM breccia are discussed in detail including data on the mineralogy, bulk chemistry, organics, and oxygen isotopes. Petrographic study shows that the white clast consists of two areas with different granoblastic textures: (1) a coarse-grained (average grain size: ~200 μm) and (2) a fine-grained lithology (average grain-size: ~20 μm). The Fa-content of olivine in the clast is the same as Fa within olivine from Rumuruti (R) chondrites (Fa: ~38 mol%); however, the concentrations of the elements Ni and Ca in olivine are significantly different. The fragment also contains Ca-rich pyroxene, ~An_{30-38}-plagioclase/maskelynite, Cr-rich spinel, several sulfide phases, a nepheline-normative glass, and traces of merrillite and metal. The occurrence of maskelynite and nepheline-normative amorphous phase in restricted areas of the well-recrystallized rock may indicate remarkable P-T-excursions during shock metamorphism. The O-isotope composition of the clast falls below the terrestrial fractionation line (TFL), lying in the field of CM chondrites and is significantly different from data for bulk R chondrites. The study of the soluble organic matter revealed a highly-oxidized carbon chemistry and organomagnesium compounds reflecting high temperature and pressure processes.

1. Introduction

CM (Mighei-type) chondrites are frequently impact breccias, sometimes very complex ones, in which lithic clasts and mineral fragments showing various degrees of aqueous alteration and/or possibly originating from different parent bodies may be mixed together (e.g., Metzler et al., 1992; Bischoff, 1998; Bischoff and Schultz, 2004; Bischoff et al., 2006, 2017, 2018; Isa et al., 2014; Kerraouch et al., 2018; Ebert et al., 2018). As typical for breccias, all types of clasts are embedded in a fine-grained clastic matrix (e.g., Metzler et al., 1992; Bischoff et al., 2006). However, considering clasts exhibiting different degrees of aqueous alteration, the location, timing, and conditions (e.g., fluid compositions, temperatures) and in particular the chronological relationships to brecciation are still controversial (e.g., Rubin and Wasson, 1986; Metzler et al., 1992; Metzler and Bischoff, 1996; Bischoff et al., 2006; Brearley, 2006). Although it is well-known that CM chondrites as a class contain fragments that experienced various degrees of alteration (e.g., Metzler et al., 1992, Lindgren et al., 2013; Hewins et al., 2014), in general CM chondrites are frequently discussed as being homogeneous rocks. They are usually classified by the degree of aqueous alteration of the most abundant lithology in a (sometimes small) thin section (e.g. CM2.3; Rubin et al., 2007; Verdier-Paoletti et al., 2017), instead of alternatively giving the whole range of occurring altered clasts (e.g., CM2.2–2.7; Bischoff et al., 2017; Lentfort et al., 2019), which would be in accordance with the classification of ordinary and R chondrite breccias.

The occurrence of CM-like clasts in other chondritic and achondritic meteorite breccias is well-documented (e.g., Fodor and Keil, 1976; Fodor et al., 1976; Zolensky et al., 1992, 1996; Bischoff et al., 2006; Patzek et al., 2018); however, reports on the occurrence of foreign

* Corresponding author.
E-mail address: kerrimene@gmail.com (I. Kerraouch).

https://doi.org/10.1016/j.chemer.2019.06.002
Received 30 March 2019; Received in revised form 2 June 2019; Accepted 6 June 2019

clasts in CM chondrites are rare (Isa et al., 2014; Bischoff et al., 2018; Kerraouch et al., 2018; Ebert et al., 2018). Ebert et al. (2018) report on an achondritic fragment of pyroxene with distinct exsolution lamellae within a CM chondrite. This fragment has a fractionated REE pattern with a distinct enrichment of the heavy REE and an O-isotopic composition similar to that of the silicate inclusions within the Tucson iron meteorite (Ebert et al., 2018).

Earlier, Isa et al. (2014) analyzed a "chondrule-free" clast in Murchison, which has a sharp boundary to the host meteorite and suggested that it originated from the R chondrite parent body. Reported olivine compositions were in the equilibrated R chondrite range ($Fa_{36–37}$) and the grains are ~10–100 μm in apparent size, usually attached to sulfides. They also reported that oxides consist of Al-rich chromite and that sulfide phases include stoichiometric FeS (either troilite or pyrrhotite) and monosulfide solid solution (mss – which at low temperatures consists of a fine intergrowth of FeS and pentlandite). Coarse-grained pentlandite was not found, but one 10 μm-sized metallic Fe-Ni grain was reported (Isa et al., 2014). We reinvestigated this same clast (Bischoff et al., 2018; Kerraouch et al., 2018) and demonstrated that the clast is not related to R chondrites. In this study the main mineralogical characteristics of this clast are summarized in detail including data on the bulk chemistry, organics, and oxygen isotopes, in order to properly understand its characteristics and affinities.

2. Sample and analytical techniques

2.1. Polished sections

For the mineralogical studies several polished sections from the white clast in Murchison (CM2; Fig. 1) were prepared at E-beam laboratories of the Astromaterials Research and Exploration Science (ARES) Division at NASA-Johnson Space Center (JSC, USA) and at the Institut für Planetologie (Universität Münster, Germany).

At JSC one polished thick section (A) was prepared consisting of two small pieces (~1 mm in size) of the clast (A1 and A2; Figs. 2 and 3). One piece shows the boundary between the clast and the CM2-Murchison host (A1) and the other represents only the clast (A2). The polished section (B) is a thin section (PL17153 with the clast of approximately 1 x 2 mm in size) and was prepared and studied at the Institut für Planetologie in Münster.

2.2. Optical and scanning electron microscopy

The petrographic study of the thin section was carried out by optical microscopy in transmitted and reflected light using a ZEISS polarizing microscope (AXIOPHOT). Images in transmitted (plane and crossed polarizers) and reflected light were taken with an integrated Olympus XC30-camera. The software analysis pro by Olympus was used for the documentation of the results.

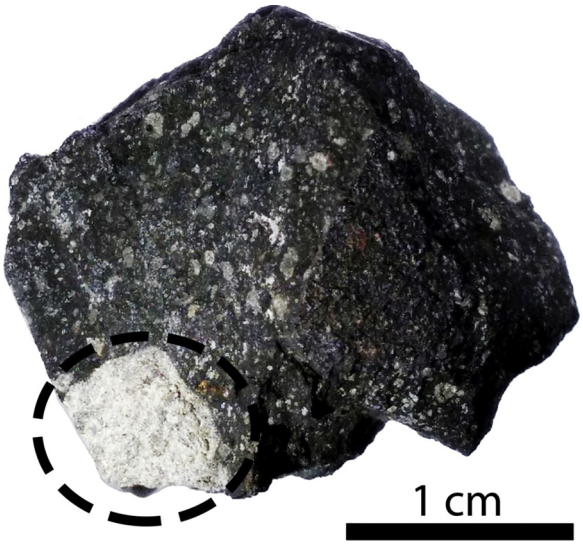

Fig. 1. White clast in the CM2 chondrite breccia Murchison.

Imaging and characterization of the rock constituents were partly done using a JEOL 7600-FE field emission SEM at ARES (JSC), and with a JEOL 6610 L V scanning electron microscope (SEM) and at the Interdisciplinary Center for Electron Microscopy and Microanalysis (ICEM, Münster). Images were taken using backscattered electrons (BSE). Using the SEM in Münster for quantitative analysis, the beam current constancy was controlled by a Faraday cup and samples and appropriate mineral standards were measured at an excitation voltage of 20 kV. Standard (Astimex) olivine (Mg, Fe, Si), jadeite (Na), plagioclase (Al), sanidine (K), diopside (Ca), rutile (Ti), chromium-oxide (Cr), rhodonite (Mn), and pentlandite (Ni) were used as natural and synthetic standards. For these EDS analyses the INCA analytical program provided by Oxford Instruments was used.

2.3. Electronic microprobe

Mineral grains in the section (A) were analyzed for major elements using a JEOL 8530-FE electron microprobe at ARES/JSC, with a focused beam. We used natural mineral standards, and applied corrections for absorption, fluorescence, and atomic number effects using the JEOL online PAP program.

Quantitative mineral and bulk chemical analyses of section B were obtained using a JEOL JXA 8530 F electron microprobe (EPMA) at the Institut für Mineralogie (Münster), which was operated at 15 kV and a probe current of 15 nA. Natural and synthetic standards were used for wavelength dispersive spectrometry. Jadeite (Na), kyanite (Al), sanidine (K), chromium oxide (Cr), San Carlos olivine (Mg), hypersthene (Si), diopside (Ca), rhodonite (Mn), rutile (Ti), fayalite (Fe), apatite (P), celestite (S), cobalt oxide (Co), and nickel oxide (Ni) were used as standards for bulk and mineral analyses. The chemical analyses of different mineral phases within the fragment were performed using a defocused beam of variable sizes (5–10 μm). The measurement time was 7.5 s for Na and K (to prevent evaporation) and 15 s for the other elements. Matrix corrections were made according to the Φρ (z) procedure (Armstrong, 1991).

2.4. LA-ICP-MS

Rare earth element concentrations (REEs) were measured by laser ablation inductively coupled mass spectrometry (LA-ICP-MS) at the Institute of Mineralogy, University of Münster, utilizing an Analyte G2 Excimer Laser Ablation System coupled to a Thermo Scientific ELEMENT 2™ ICP-MS. The laser operates at a wavelength of 193 nm and the measurements were taken with a pulse length of 4 ns and a repetition rate of 5 Hz at a total energy of 3 J/cm^2 with a spot size of 100 μm. The background was measured for 20 s and peaks were measured for approximately 40 s. To ensure correct measurements, the USGS reference glass BIR-1 G was analyzed sequentially and compared to previous measurements and publications on the GeoRem homepage (Klaus Peter Jochum et al., 2005 (georem.mpch-mainz.gwdg.de)). All obtained concentrations are in the range of the published values. NIST 612 was analyzed as an external reference material and Si was used as an internal reference element (values stem from previous EPMA measurements). The results were reduced using the *Glitter* software by manually defining the background and the sample.

2.5. Oxygen isotope analyses

The oxygen isotopic compositions of olivine grains within the xenolithic clast from Murchison were obtained using the IMS1280-HR ion probe at the University of Heidelberg (Table 2). ^{16}O, ^{17}O, and ^{18}O were

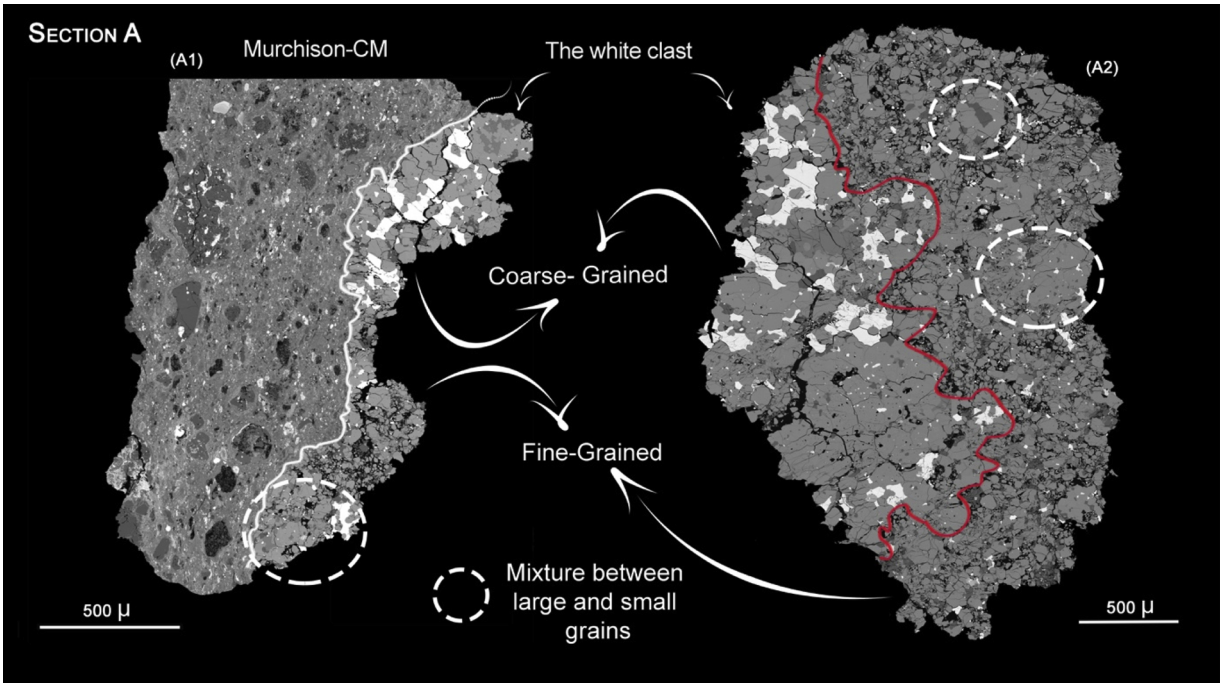

Fig. 2. Overview of the two pieces present in the thick section A. The white clast consists of areas with a coarse-grained and a fine-grained texture. The white line in the fragment on the left-hand side (A1) indicates the sharp boundary between the fragment and the Murchison host. The red line within the other fragment demonstrates the boundary between the coarse and fine-grained units (A2). Images in back-scattered electrons (For interpretation of the references to colour in this figure legend, the reader is referred to the web version of this article).

analyzed utilizing a 10 keV Cs^+ primary ion beam with a beam current of 4–5 nA sputtering an analyses area of 6 x 6 µm (20 × 4s). Pre-sputtering of 8 x 8 µm before each analysis was carried out to increase secondary ion yields. Negative ions were collected by Faraday cups and corrected for IMF by analyzing in-house San Carlos standard olivine and pyroxene grains, which had been pre-measured by laser fluorination mass spectrometry at the University of Göttingen. Baselines were determined separately with 400 s integration time. The Mass Resolution Power (MRP) was set to ~7000 for ^{17}O and ~2500 for ^{16}O and ^{18}O. Charge compensation was accomplished using the Normal-incidence Electron Gun (NEG). Results are reported in δ-notation versus VSMOW with a typical precision of ± 0.3‰ in $\delta^{18}O$ and ± 0.5‰ in $\delta^{17}O$.

A bulk sample of ~1 mg was analyzed by laser fluorination in combination with gas source mass spectrometry (Sharp, 1990) in order to measure the bulk oxygen isotope composition. These data were normalized to the composition of San Carlos olivine ($\delta^{17}O_{VSMOW2}$ = 2.715‰, $\delta^{18}O_{VSMOW2}$ = 5.220‰; see Pack et al., 2016).

2.6. Modal abundance and calculation of bulk composition

The mineral abundances within the clast were obtained using X-ray

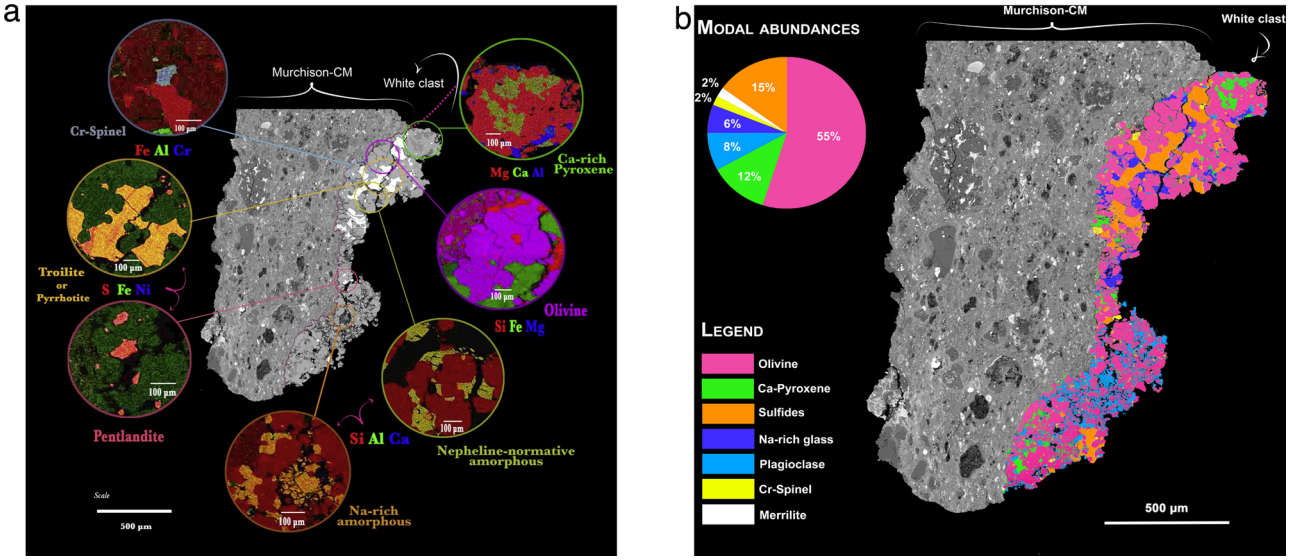

Fig. 3. (3a). Back-scattered electron image of the clast within Murchison and composite maps of areas of interest representing distinct mineral phases. Locally, the plagioclase has been transformed into maskelynite. The color figure can be seen in the online version. (3b). Mineralogical map showing the distribution of various phases within the fragment (colored area) and giving the modal abundance in the upper left.

elemental maps and the software "ImageJ". Sulfides were determined using S elemental maps and the modal abundance of olivine by Si and Mg elemental maps. Mg, Ca, and Si elemental maps were used for pyroxene and Si, Al, and Ca for feldspar. To identify Cr-spinel, Fe, Al, and Cr maps were used (Fig. 2). The modal abundances were calculated based on counting statistics. The bulk composition of the clast was calculated by combining the results of the modal abundance of each mineral phase with the appropriate compositional EMPA data. A density correction was performed.

2.7. Soluble organic matter analysis

A 4 mg fragment of the material was crushed in a mortar with 150 µl of ultrapure LC/MS grade methanol solvent. To avoid external organic contamination the fragment was washed intensively with the solvent prior to crashing. Fourier transform ion cyclotron resonance mass spectrometry (FT-ICR-MS) was undertaken in negative electrospray ionization mode (ESI) following standard operation procedures as described previously by Schmitt-Kopplin et al. (2010, 2012) with 1500 averaged scans. The polar, protic solvent extraction (methanol) and mild ESI-ionization preferentially extracted and ionized polar, oxygenized molecules. The software package "Data Analysis 4.0″ (Bruker, Bremen, Germany) was used for data processing and all molecular formulas were assigned by custom-made software (NetCalc network), as described by Tziotis et al. (2011). All molecular formulas were classified into CHO, CHNO, CHOS, CHNOS, and CHOMg molecular series, which were visualized in their abundances using the class-selective van Krevelen diagrams (Schmitt-Kopplin et al., 2010, 2012; Hertkorn et al., 2015; Ruf et al., 2017).

3. Results

3.1. Petrography and mineralogy

The white clast had a sharp boundary with the Murchison host lithology (Figs. 1, 2 and 4) and consists of two areas with different granoblastic textures: (1) a coarse-grained lithology (average grain size: ~200 µm; mainly present in thick section A) and (2) a fine-grained lithology (average grain-size: ~20 µm; within all sections, but mainly in thin section B). A mixture of both textural types is present in some portions of the studied sections (Fig. 2). All subsamples show a well-recrystallized texture. Thin section "B" mainly consists of the fine-grained lithology and has well-recrystallized areas with 120° triple junctions between adjacent crystals and an eye-catching area that may represent a relic chondrule (Fig. 5). The clast studied in this section essentially consists of silicates (mainly olivine, Ca-pyroxene, and plagioclase), a few sulfides (compared with their abundance in the coarse-grained lithology in section A; Fig. 2) and minor Cr-spinel. Additionally, one small (< 1 µm) PGE-rich particle was detected in thin section B, and in thin section A some tiny metal grains (probably awaruite (Ni_3Fe)) enclosed in pentlandite are present (Fig. 5c). The clast has a sharp boundary with the Murchison host meteorite (Fig. 4) and no indication of aqueous alteration (including at the boundary) was detected. Mineral compositions and the bulk composition of the clast are summarized in Table 1.

It was apparent from the element mapping (Fig. 2; area A1) that olivine is the dominant phase in the clast at about ~55 vol% (Fig. 3b). Within the coarse-grained lithology olivine is characterized by large, fractured, anhedral crystals. Small olivine grains in the fine-grained areas sometimes have a rounded shape and are enclosed in plagioclase/maskelynite (Fig. 5b). The composition of the olivine is uniform (equilibrated) across the entire clast at $Fa_{37.9 \pm 0.4}$, with low mean Ni values (NiO = 0.11 ± 0.04 wt%; Table 1) and high mean CaO concentrations (0.3 wt%; Table 1) compared to R-chondrites. In most cases the NiO concentration in olivine is below 0.10 wt%. High-Ca pyroxene ($Fs_{10.9 \pm 0.7}$, $En_{40.6 \pm 0.6}$, and $Wo_{48.5 \pm 1.1}$; Table 1) is present at ~12 vol

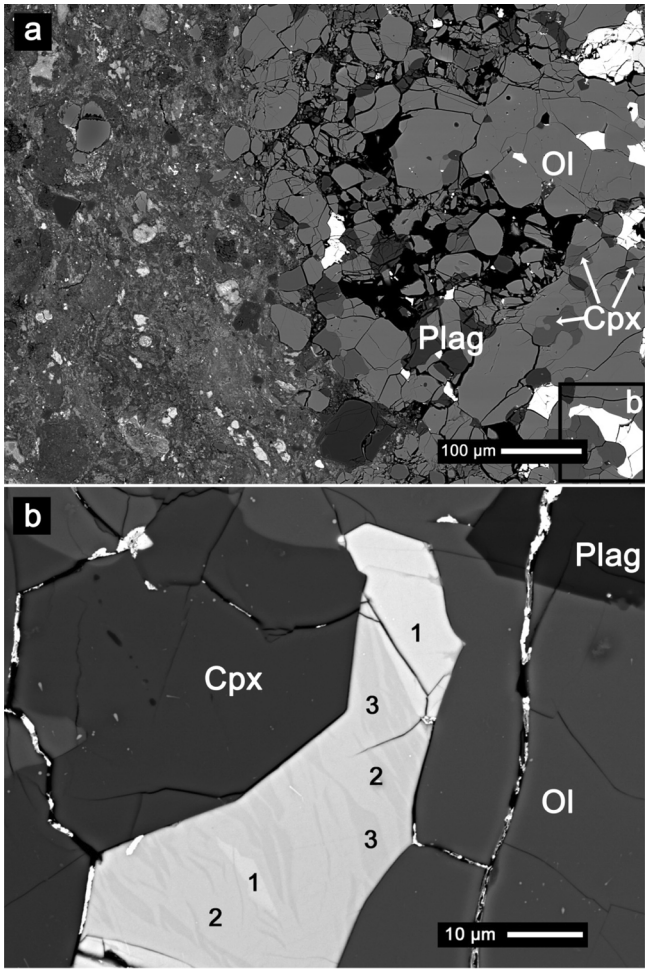

Fig. 4. (a) The sharp boundary between the clast and the Murchison host breccia (left-hand side). Note the brecciated appearance within the fragment with abundant pores and fractures (black) and plagioclase (dark grey). In the lower right-hand corner, a sulfide assemblage is visible described in detail in (b). (b) Fine-grained paragenesis of three different sulfide minerals from the coarse-grained lithology. The white phase is pentlandite (1), whereas the remaining fine-grained intergrowth probably consists of troilite (2) and pyrrhotite (3). The cracks contain some Au from sputtering. Ol = olivine; Cpx = Ca-pyroxene; Plag = plagioclase. Images in back-scattered electrons.

% - less abundant than olivine and preferentially present in the coarse-grained lithology. The well-equilibrated pyroxene is typically enclosed in olivine as anhedral crystals (see Fig. 3, upper right). Plagioclase (or maskelynite; 8 vol%) is preferentially present in the lithology with a fine-grained texture and is slightly unequilibrated ($Ab_{61.1 \pm 3.0}$, $An_{38.1 \pm 3.1}$, and $Or_{0.8 \pm 0.5}$). Raman spectroscopy of section A revealed that in some areas of the clast the plagioclase is isotropic and must have been transformed to maskelynite (see more details below). An unknown Na-rich phase is present in one thick section (~6 vol%) whose chemical composition is similar to nepheline (Table 1), although the calculated structural formula deviates from stoichiometric nepheline. No peaks for nepheline or other mineral phases could be detected in this phase by Raman spectroscopy (Fig. 6). Thus, the Na-rich constituent must be amorphous.

Cr-spinels (~2 vol%) are also preferentially present in the fine-grained-areas of the clast and are significantly variable in composition (Cr_2O_3: 24–46 wt%). Most of the Cr-spinels in the Murchison clast have relatively low TiO_2-concentrations (~3 wt%; range: 1.3–5 wt%) and high Al_2O_3 (> 25 wt%) compared to R chondrites. At least three different sulfides are present in the clast. Pentlandite (~6 vol%), troilite and pyrrhotite (together ~9 vol%) are present in the coarse-grained

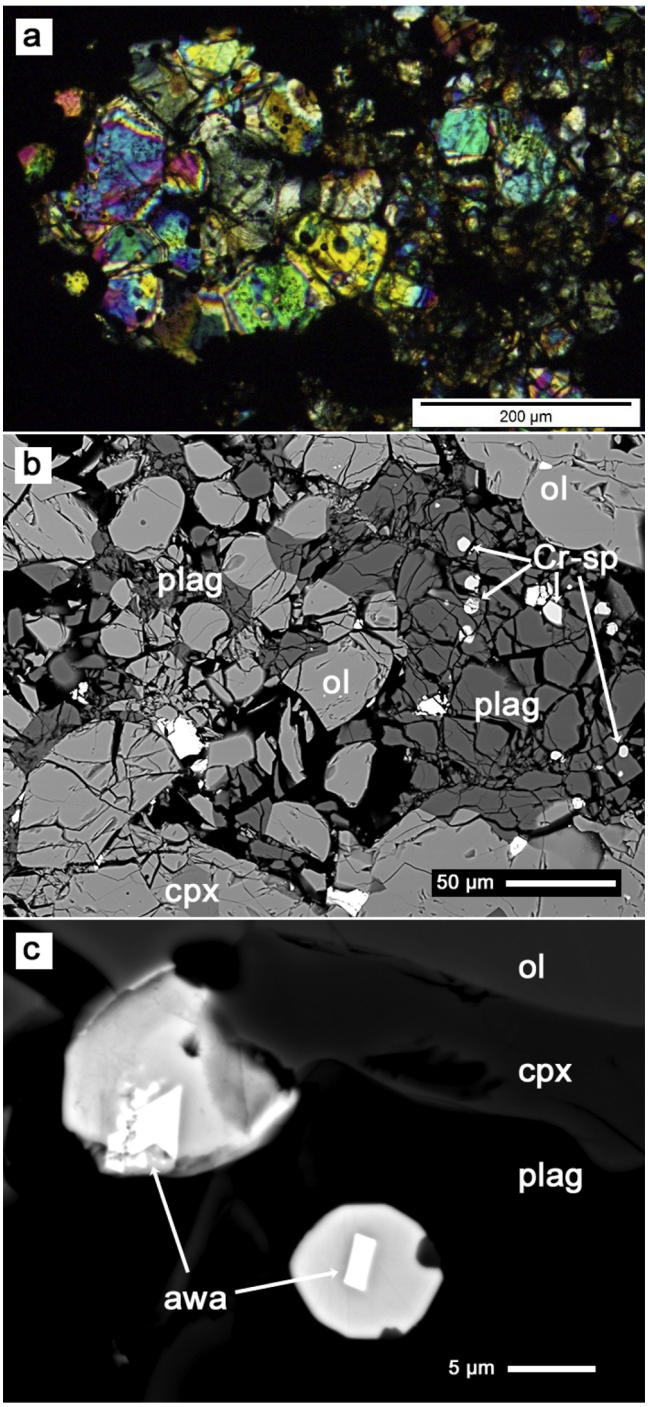

Fig. 5. (a) A conspicuous area in thin section B that may represent a relic olivine-rich chondrule, whereas the entire thin section shows a recrystallized texture. Image in polarized light; crossed nicols; (b) fine-grained area with abundant plagioclase/maskelynite (plag) mainly enclosing olivine (ol); (c) tiny metal-grains of awaruite (awa) enclosed in pentlandite; ol = olivine; cpx = Ca-pyroxene; plag = plagioclase/maskelynite; Cr-sp = Cr-spinel. Images (b) and (c) in back-scattered electrons.

lithology (Fig. 4; Table 1), whereas pentlandite is by far the major sulfide in the fine-grained-textured lithology. The modal abundance of all sulfides totals 15 vol%. Minor merrillite (~2 vol%) was also detected (Table 1).

From the modal abundances of plagioclase/maskelynite (~$An_{38.1}$), the Na-rich amorphous phases, and the Ca-pyroxene, relatively high bulk concentrations of Ca, Al, and Na were calculated from the modal mineralogy of section A1 (Fig. 2) (Table 1). These calculated values are supported by bulk chemical analysis of the clast in thin section B by quantitative SEM-EDS (Table 1).

3.2. Oxygen isotopes

The measured O-isotope data are given in Table 2. These data are indistinguishable from the SIMS data on clast olivines, fall below the terrestrial fractionation line (TFL) and are in the field of CM chondrites (Fig. 7). They are distinct from data for bulk brachinites (Greenwood et al., 2012) and for bulk R chondrites (Bischoff et al., 2011).

3.3. Rare earth elements

The REE concentrations measured from six different spots in the clast are listed in Table 3 and plotted in Fig. 8. The spots are randomly-distributed on silicate- rich areas in order to reveal the composition of the bulk silicates. The different spots have variable REE concentrations ranging from La = 0.1 x CI (spot d) to La = 2.85 x CI (spot f). Two spots have a negative Eu anomaly ("b" and "c") whereas two other spots have a positive Eu anomaly ("d" and "e"). The spots "a-e" are enriched in the HREE (heavy rare earth elements) compared the LREE (light rare earth elements). The only exception is spot "f", which has a nearly flat REE pattern with a weak positive Eu anomaly, and a slight enrichment of the LREE compared to the HREE. On average, the white clast has a chondritic pattern from La = 0.88 x CI to Lu = 2.20 x CI and with a slight enrichment of the HREE compared to the LREE (Fig. 8).

3.4. Solvent soluble organics

Ultrahigh-resolution mass spectrometry enables a description of thousands of exact masses and their relative abundance out of highly complex organic mixtures. These mass signals are converted into their corresponding formula using the elements C, H, O, N, S and Mg and can be visualized in van Krevelen diagrams, as presented by previous studies of Murchison soluble organic matter (Schmitt-Kopplin et al., 2010). The analysis of the Murchison white clast reveals a lower number of CHNOS elemental compositions (5800) with a lower proportion of sulfurized compounds as compared to typical Murchison matrix (13.000 formula as shown in Fig. 9 A–D). Detailed analysis of the specific compounds in the clast showed the presence of highly-oxygenated and N-containing compounds (Fig. 9 C–D). Further investigation showed a much higher abundance of organomagnesium molecules in the clast relative to Murchison fine-grained matrix, probably reflecting a higher degree of thermal metamorphism experienced by the clast (Fig. 10).

4. Discussion

4.1. Classification of the clast

The REE abundance of the white clast has an approximate bulk chondritic composition (e.g., Lodders and Fegley, 1998). The REE chondrite pattern (Fig. 8) indicates a chondritic genesis and excludes formation and processing on a differentiated parent body. This contention is well-supported by the O-isotope composition that indicates a close relationship to CM chondrites (Fig. 7). As a consequence of the O-isotope data in particular, a relationship to R chondrites, as earlier suggested by Isa et al. (2014), can be ruled out.

Considering the very low abundance of Fe,Ni-metal and the high Fa-content of olivine, the rock must have been formed or thermally processed in an oxidizing environment. Such an origin is also supported by the data on the highly-oxidized soluble organic compounds (Fig. 9). The clast has a well-recrystallized texture and is rich in olivine (~Fa_{38}) which is well-equilibrated as is the coexisting pyroxene (diopside; ~$Fs_{11}Wo_{40}$). This olivine composition is very near the value for olivine

Table 1
Mean chemical composition of the main phases of the metamorphosed fragment in the Murchison breccia. (a) silicates and oxides; (b) sulfides. All data in wt%; Number in brackets = number of measurements; nd = not detected; na = not analyzed; bdl = below detection limit; the calculated bulk composition was obtained by considering the modal abundances of the detected phases and their chemical composition. *SEM-EDS and normalized to 100; **large-scale area of thin section B measured by SEM-EDS and normalized to 100 (contains traces of K, P, and Co); #analyzed and calculated as SO_3.

a	Olivine (100)			Ca-pyroxene (30)			Plagioclase (16)			Na-rich glass (3)			Cr-spinel (3)			Merrillite (4)*			Bulk	
	wt%		std	wt%		std	wt%		std	wt%		std	wt%		std	wt%		std	calculated	measured**
Na_2O	bdl			0.63	±	0.06	7.1	±	0.54	17.5	±	0.51	nd			2.81	±	0.07	1.76	0.96
MgO	30.6	±	0.33	13.9	±	0.33	0.10	±	0.13	0.02	±	0.01	3.9	±	0.16	3.31	±	0.11	18.4	22.9
Al_2O_3	bdl			2.56	±	0.66	26.3	±	0.77	34.5	±	0.08	22.4	±	4.12	bdl			5.0	3.3
SiO_2	36.5	±	0.29	51.9	±	0.56	58.5	±	0.22	44.6	±	0.68	0.06	±	0.01	0.23	±	0.04	33.5	33.5
S	bdl			bdl				bdl		nd				bdl			bdl		5.4	5.6#
P_2O_5	bdl			bdl			bdl			nd			bdl			46.3	±	0.26	0.96	nd
K_2O	nd			bdl			0.16	±	0.08	2.79	±	0.13	nd			0.08	±	0.05	0.18	bdl
CaO	0.31	±	0.02	23.1	±	0.57	7.7	±	0.32	1.45	±	0.04	bdl			45.9	±	0.19	4.6	1.72
TiO_2	bdl			0.84	±	0.22	0.08	±	0.02	0.02	±	0.01	4.1	±	0.83	0.10	±	0.06	0.21	0.09
Cr_2O_3	0.04	±	0.02	0.91	±	0.17	bdl			nd			32.6	±	3.02	bdl			0.81	0.44
FeO	32.6	±	0.33	6.7	±	0.39	0.93	±	0.06	0.94	±	0.04	34.9	±	0.51	1.04	±	0.11	27.2	28.2
NiO	0.11	±	0.04	0.03	±	0.03	bdl			1.05	±	0.04	0.34	±	0.26	0.11	±	0.07	1.79	2.78
MnO	0.36	±	0.03	0.10	±	0.02	bdl			bdl			0.27	±	0.04	bdl			0.22	0.23
Total	100.5	±	0.44	100.6	±	0.58	100.9	±	0.51	102.9	±	1.42	98.6	±	0.15	100.0				
Fa	37.9	±	0.44																	
Fo	62.1	±	0.44																	
Fs				10.9	±	0.65														
En				40.6	±	0.61														
Wo				48.5	±	1.11														
An							38.1	±	3.08											
Ab							61.1	±	3.04											
Or							0.8	±	0.50											

b	pentlandite* (3)			troilite* (3)			pyrrhotite* (2)		
	wt%		std	wt%		std	wt%		std
Fe	38.1	±	0.34	62.6	±	0.29	61.0	±	0.03
S	33.6	±	0.07	36.9	±	0.14	38.5	±	0.06
Ni	27.5	±	0.54	0.11	±	0.10	0.18	±	0.04
Co	0.81	±	0.15	0.38	±	0.09	0.35	±	0.04

Table 2
The oxygen isotopic compositions of olivine grains and of the bulk rock of the xenolithic clasts from the Murchison breccia. The olivine data were obtained using the ion probe, whereas the bulk composition was analyzed by laser fluorination mass spectrometry.

	$\delta^{18}O$	2σ	$\delta^{17}O$	2σ	$\Delta'^{18}O$
Clast Ol - 1	6.67 ± 0.14		0.50 ± 0.27		−2.97
Clast Ol - 2	7.26 ± 0.12		0.58 ± 0.24		−3.20
Clast Ol - 3	7.15 ± 0.12		0.42 ± 0.26		−3.30
Clast bulk	6.85 ± 0.40		0.46 ± 0.20		−3.16

in Murchison artificially heated to 1200 °C (Tonui et al., 2014). Based on texture and mineralogy (olivine, pyroxene) the clast is of high petrologic type 6 (e.g., Van Schmus and Wood, 1967; Brearley and Jones, 1998). However, it cannot be ruled out that some recrystallization observed within olivine is the result of moderate shock metamorphism (mosaicism (S4); Stöffler et al., 1991; Bischoff and Stöffler, 1992)

4.2. Mineralogical comparison with R chondrites and other rocks

As mentioned above, Isa et al. (2014) suggested that this clast in Murchison was a fragment of the Rumuruti parent body. The Fa-content of olivine in the clast is indeed the same as that for R chondrites (Fa: ~38 mol%). However, the concentrations of Ni and Ca in olivine are somewhat different (Tab. 5; Fig. 11) than for typical R's. The olivine in the Murchison clast has low NiO (mostly < 0.1 wt%), whereas typical olivine in R chondrites has 0.2-0.4 wt% NiO (Bischoff et al., 2011; Fig. 11). Also, the olivine in the clast has ~0.3 wt% CaO, which is significantly higher than observed in Rumuruti chondrites (e.g., Bischoff et al., 2011). The common plagioclase in R chondrites is quite albitic (< An_{12}); however, in the Murchison clast most plagioclase/maskelynite grains are close to An_{38} and are slightly unequilibrated (Fig. 12). The compositional data for olivine, pyroxene, and many plagioclases in the clast are similar to those in the brachinite EET 99,402 (Gardner-Vandy et al., 2013); however, the composition of spinel is significantly different. Cr-rich spinels within this clast are variable in composition (Cr_2O_3: 24–46 wt%), whereas in EET 99,402 chromite with 51% Cr_2O_3 occurs. Compared with spinel-group minerals in R chondrites, most of the grains within the Murchison clast have relatively low TiO_2-concentrations (~3 wt%; range: 1.3–5 wt%) and high Al_2O_3 (> 25 wt%). Intergrowths of at least three sulfides (pentlandite, troilite, and pyrrhotite; Fig. 10c) have been observed, which may result from exsolution of pentlandite from troilite or monosulfide solid solution as the temperature dropped below the stability field for a high temperature phase. Finally, the Murchison clast contains a nepheline-normative component (described as albite in Isa et al. (2014) and determined by Raman spectroscopy in this study to be amorphous) that has never been observed in any R chondrite.

In summary, the well-equilibrated olivines with the appropriate Fa contents of 37–40 mol%, the occurrence of abundant Ca-pyroxene, and the recrystallized texture within the Murchison clast is consistent with an R6 classification (e.g., Imae and Zolensky, 2003; Berlin and Stöffler, 2004; Bischoff et al., 2011; Brearley and Jones, 1998). However, the low NiO-concentration (mostly < 0.1 wt%) and high CaO content (0.3 wt%) in olivine, the oxygen isotopic compositions of olivine and the bulk clast, the chemical compositions of Cr-spinel and plagioclase do not support a genetic relationship between the clast and R

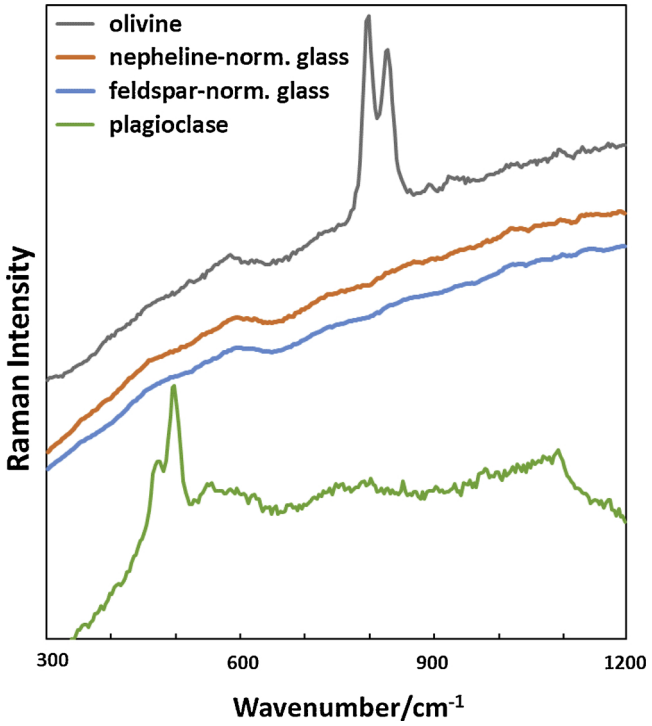

Fig. 6. Raman spectra of olivine, nepheline-normative and feldspar-normative glass from the coarse-grained lithology in the thick section A, and plagioclase from the fine-grained lithology in the thin section. Olivine is identified by two characteristic peaks at ~820 cm^{-1} and ~840 cm^{-1} and plagioclase by two peaks at ~481 cm^{-1} and ~510 cm^{-1}. The feldspar- and the nepheline-normative glasses are featureless with increasing intensity due to increase of fluorescence. The spectra are not corrected for the background emission.

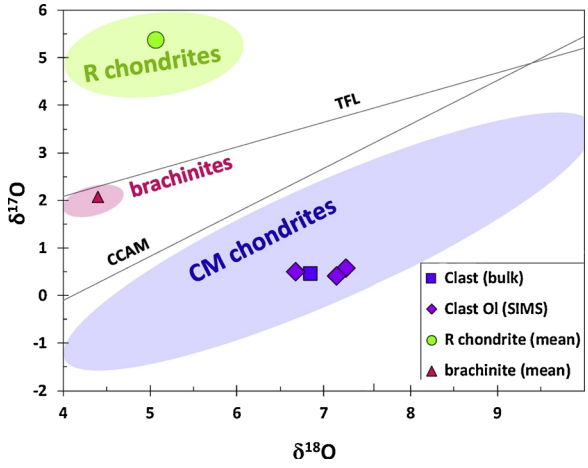

Fig. 7. Oxygen isotope composition of the bulk clast and of individual olivine grains. The mean data for brachinites and R chondrites are from Greenwood et al. (2012) and Bischoff et al. (2011), respectively. The data for CM chondrites are from Clayton and Mayeda (1999). TFL = Terrestrial Fractionation Line; CCAM = Carbonaceous Chondrite Anhydrous Mineral line.

chondrites (compare for R chondrite: e.g., Rubin and Kallemeyn, 1994; Brearley and Jones, 1998; Greenwood et al., 2000; Bischoff et al., 2011).

4.3. Origin and formation of the Murchison clast

From our previously-mentioned results, several points are important for the discussion about the origin and the formation processes of the Murchison clast: (a) The O-isotope data indicate that the clast is related to CM chondrites or formed within a similar environment. Thus, the possible occurrence and the influence of water/ice during the parent body evolution of the clast should be considered. (b) The rock is well-recrystallized, but represents two different lithologies (having coarse and fine-grained textures (Figs. 2–4)). (c) The texturally different lithologies also contain different mineral phases (Fig. 3). Only olivine has the same composition in both lithologies. (d) Surprisingly and unexpectedly, the coarse-grained, well-recrystallized lithology contains a nepheline-normative amorphous phase glass and locally minor maskelynite in paragenesis with Cr-spinel and Ca-rich-pyroxene. (e) Plagioclase (~An_{38}) is predominantly present within the fine-grained lithology and is heavily-fractured. (f) The sulfides show different mineralogies and compositions in both parts: Pentlandite, troilite, and pyrrhotite occur within the coarse-grained lithology and pentlandite is by far the main sulfide in the fine-grained lithology (Figs. 2–4).

Table 3
CI-normalized values of the concentrations of the REE of various areas of the metamorphosed clast in the Murchison breccia. The data obtained by LA-ICP-MS were normalized to CI chondrites (Barrat et al., 2012).

CI norm	a	b	c	d	e	f	average
La	0.153	0.787	0.834	0.138	0.528	2.851	0.882
Ce	0.183	1.150	1.333	0.232	0.442	2.833	1.029
Pr	0.204	1.451	1.560	0.164	0.516	2.549	1.074
Nd	0.237	1.573	2.198	0.026	0.379	2.198	1.102
Sm	0.141	2.229	2.725	0.044	0.830	2.412	1.397
Eu	0.459	0.215	0.478	0.546	2.014	3.242	1.159
Gd	0.301	2.039	2.476	0.109	0.291	1.796	1.169
Tb	0.147	2.480	2.933	0.059	0.827	2.080	1.421
Dy	0.409	2.244	2.992	0.080	1.169	2.283	1.530
Ho	0.366	2.226	2.491	0.207	1.272	2.173	1.456
Er	0.639	2.169	2.470	0.620	1.500	2.108	1.584
Tm	0.859	1.565	2.748	0.905	2.481	1.718	1.712
Yb	1.208	2.381	2.857	1.226	2.143	2.500	2.053
Lu	1.489	2.672	2.366	1.527	2.672	1.718	2.074

Consequently, these apparently inconsistent observations on the mineralogy of the two coexisting lithologies lead to some important questions: (1) Why do two distinct lithologies coexist in the Murchison clast? (2) Why do we locally find nepheline-normative glass and maskelynite within a well-recrystallized rock fragment?

The clast in Murchison is certainly not a heated and dehydrated "normal" CM chondrite like the recently described CM-anomalous rock NWA 11,024 (Ebert et al., 2019). Brecciated meteorite fragments with completely different textures, mineralogy, and/or isotopic signatures are generally regarded as xenoliths that were incorporated into the final parent body regolith as late-arriving impact projectiles. This is particularly the case if the type of xenolith is a rare constituent of the parent host rock. This certainly could be the case here, since similar clasts in Murchison have yet not been recognized, despite the fact that and a very large number of Murchison samples have been carefully examined over the past 50 years. Murchison is by far the best-characterized CM chondrite.

Since the clast has a similar O-isotopic composition as CM chondrites, it is reasonable to conclude that it formed in a related environment. The O-isotopic composition can be seen as the primary composition as the clast shows a clear and distinct boundary to host material and no kind of aqueous alteration is present in the clast, despite its common occurrence in the host Murchison rock. An exchange of the O-isotopes with the host material is not expected and, therefore, we will consider the case that the clast originated from the CM or a CM-related parent body. The recrystallized texture and the equilibrated olivine and pyroxene indicate that the clast comes from a deep location within the parent body, essentially having olivine, pyroxene, plagioclase, and sulfide (perhaps also metals (that oxidized during annealing?)). It is possible that the parent body has been affected by impact, causing fragmentation of the rock producing the fine-grained texture, locally

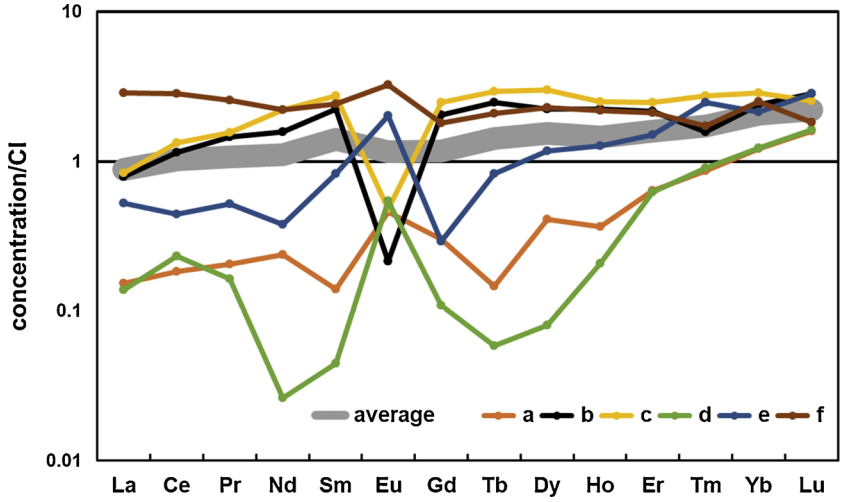

Fig. 8. REE concentrations of various areas obtained by LA-ICP-MS normalized to CI chondrites (Barrat et al., 2012). On average a flat chondritic REE pattern is obtained.

transforming the plagioclase into maskelynite due to P-T-excursions during shock metamorphism (e.g., Stöffler et al., 1991; Bischoff and Stöffler, 1992), forming the Na-rich glass, and leading to a significant increase in temperature. This suggested impact scenario is well-supported by the data of the study of the clast's organics. Organomagnesium compounds are known to be excellent witness' to record high shock and temperatures conditions (Ruf et al., 2017) and these were found in the clast in a highly oxygenated homologous structural series reflecting the impact conditions. Alternatively, we should mention that the recrystallized texture and the equilibration of olivine and pyroxene may result from annealing in a warm ejecta blanket nearer the surface.

Locally, the energy was high enough (a) to produce melt that infiltrated and percolated in parts of the solid rock, and (b) to promote crystal growth leading to the formation of the coarse-grained lithology (including formation of Ca-pyroxene and spinel). These processes are significantly assisted by the circulation of fluids in the rocks, since we know that water (and/or other fluids) play an important role in the evolution of the CM parent body(ies). Considering terrestrial

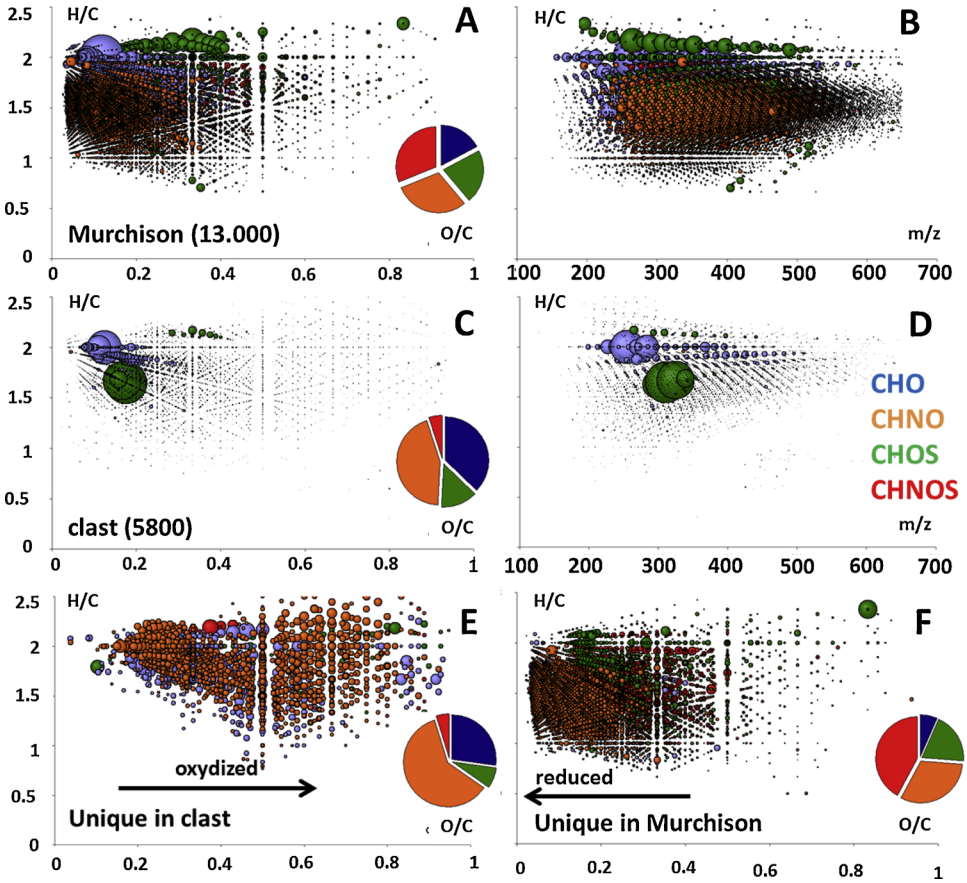

Fig. 9. van Krevelen diagrams of the soluble organic matter of Murchison (A–B) and of the clast (C–D) as well as of the compounds uniquely found in the clast (E) and Murchison (F), respectively. The color code is described in (D) and the size of the bubbles is proportional to the signals in mass spectrometry.

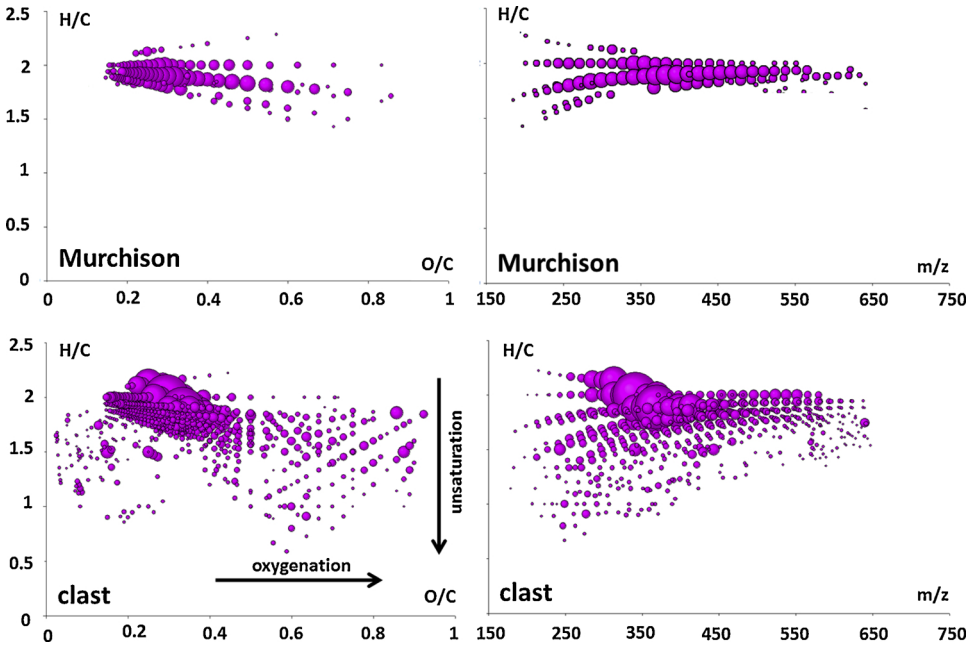

Fig. 10. van Krevelen profiles of the organomagnesium compounds in Murchison (170 formulas) and its clast (630 formulas) showing highly oxygenated and unsaturated compounds.

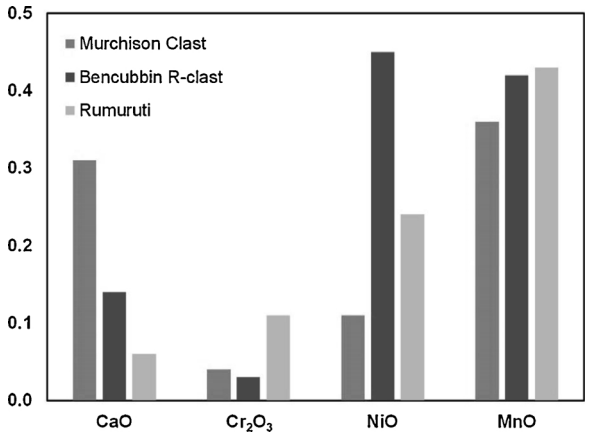

Fig. 11. The concentrations of minor elements in olivine. Olivine from the Murchison clast is significantly different from olivine in the Rumuruti chondrite (Schulze et al., 1994) and the R chondrite clast in Bencubbin (Isa et al., 2014).

environments for comparison, recent studies have shown that percolating melts may react with the mantle lithosphere, inducing enrichment in fusible components, i.e., re-fertilization via the crystallization of pyroxenes and spinel (Rampone et al., 1994; Lenoir et al., 2001; Müntener et al., 2004; Tommasi et al., 2004; Beyer et al., 2006; Le Roux et al., 2007). Considering this comparison with terrestrial mantle analogues further, experimental studies show (e.g., Hier-Majumder et al., 2004; Demouchy et al., 2007; Costa and Chakraborty, 2008) that the incorporation of water in nominally anhydrous minerals (for example olivine) or the presence of interconnected small melt fractions also enhance diffusion, favoring recovery of dislocations (Karato et al., 1993), recrystallization (Avé-Lallemant and Carter, 1970; Jung and Karato, 2001b), and grain growth (Karato, 1989). This scenario is consistent with studies of mantle xenoliths and peridotite massifs, which suggest that melt percolation under both dynamic and static conditions may significantly modify the microstructure of mantle rocks (e.g. Vauchez and Garrido, 2001; Tommasi et al., 2006, 2008; Le Roux et al., 2008; Soustelle et al., 2009). Reactive melt transport may also change modal mineralogy (Le Roux et al., 2007) and produce Fe or pyroxene-enrichment, resulting in a change in the density of mantle rocks (Lee, 2003; Tommasi et al., 2004).

Percolation can produce a cryptic or modal metasomatism. In the first case, only the exchange of chemical elements occurs, whereas in the second case new minerals will be formed by a modification of the mineralogical compositions of peridotite. It is the latter type of metasomatism which is of particular interest in this comparison. The proposed impact heating triggered recrystallization and crystal growth resulting in the coarse-grained texture present in the clast.

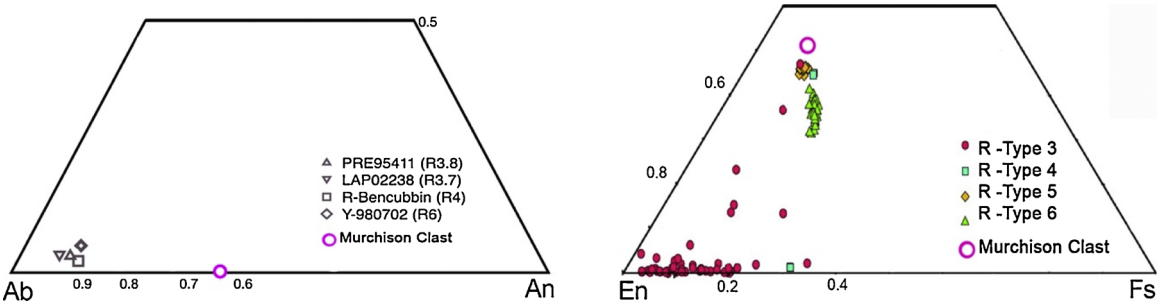

Fig. 12. The compositions of plagioclase (Isa et al., 2014) and pyroxenes in the Murchison clast compared with those of various R chondrites of different petrologic types (Type 3, 4, 5, and 6; Berlin and Stöffler (2004)). Plagioclase in the Murchison clast is distinct from plagioclase in R chondrites, which basically have albitic compositions. Ca-pyroxene is the dominant pyroxene in R chondrites of high petrologic type (see Bischoff et al. (2011) in addition).

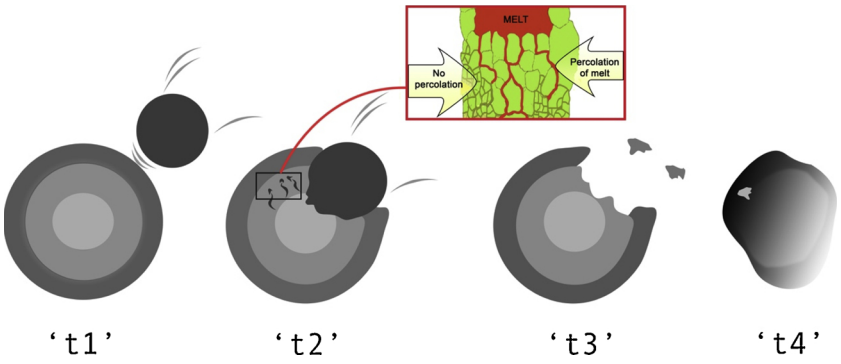

Fig. 13. Schematic portrayal of the history of the formation and origin of the white clast. t1: Collision of the parent body with another planetary body; t2: Percolation of fluids within the parent body due to impact annealing; t3: Fragmentation of the same parent body by another impact; t4: Re-accretion of different aqueously-altered clasts of different degree (CM2.0-CM2.9; compare Fig. 14) and of the white clast forming the brecciated, 2nd generation Murchison parent body.

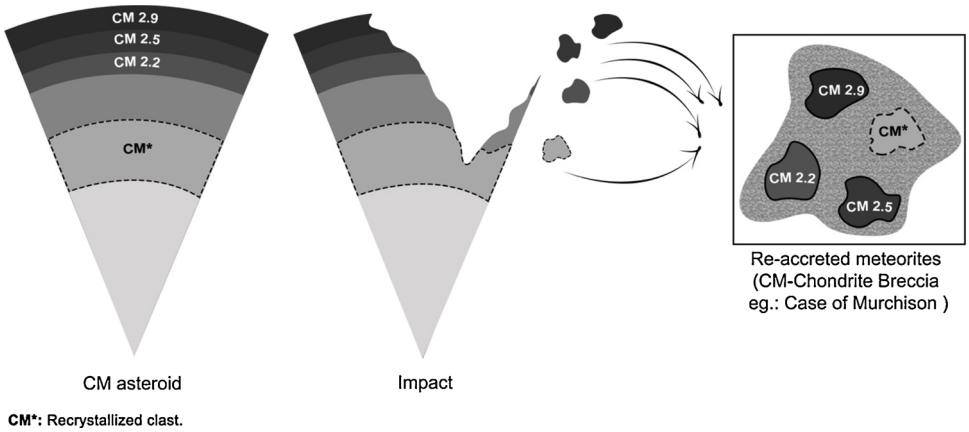

Fig. 14. Formation of lithologies with different degree of aqueous alteration and impact-related mixing of different lithologies in order to build up a genomict CM chondrite breccias.

The rock fragment (the white clast) with the two different lithologies must have been excavated by another impact prior to complete equilibration of all constituents (e.g., plagioclase) within the two lithologies and prior to recrystallization of the nepheline-normative glass and the shock-formed maskelynite. Perhaps during this same process, the white Murchison clast was mixed with other Murchison fragments exhibiting various degrees of aqueous alteration (Fig. 13).

There is another characteristic of the clast which may indicate formation at significant depth within the parent body, where partial melting may have occurred: Olivine in the clasts has high CaO contents (around 0.3 wt%). High CaO in olivine (0.3–0.45 wt%) is observed in ultramafic achondrites (e.g., ureilites; Mittlefehldt, 2006). In contrast, in type 4–6 ordinary chondrites, CaO abundance in olivine decreases with increasing petrologic type and is typically < 0.1 wt% (e.g., Dodd, 1969). However, arguing against melting is the Fe-rich olivine in the clast. Artificially-melted Murchison usually results in much more magnesian olivine (~Fa_5; Tonui et al., 2014).

4.4. Impact mixing of cognate and/or foreign clasts

As stated above, the occurrence of CM-like clasts in chondritic and achondritic meteorite breccias is well-known (e.g., Zolensky et al., 1992, 1996; Bischoff et al., 2006; Patzek et al., 2018), but reports of the occurrence of foreign clasts in CM chondrites are extremely rare (Isa et al., 2014; Bischoff et al., 2018; Kerraouch et al., 2018; Ebert et al., 2018).

The measured O-isotope composition indicates that the clast is related to CM chondrites or formed within a very similar environment. If the fragment represents a distinct lithology of the CM chondrite parent body, the clast has to be described as a "cognate" clast like other clasts in Murchison representing lithologies with different degrees of aqueous alteration or thermal metamorphism. Considering a cognate origin of the clast, the recrystallized texture, the equilibrated olivine and pyroxene, and the lack of phyllosilicates indicate formation in the deep interior of the parent body. The fragment must have been excavated by an impact and mixed with fragments of the overlying lithologies showing different degrees of aqueous alteration within the parent body surface regolith (Figs. 13 and Fig.14), possibly during a complete disaggregation of the original CM parent asteroid. We note that the great majority of large (high total mass), and therefore probably representative CMs show abundant clasts representing a considerable range of aqueous alteration (Takenouchi et al., 2013; Zolensky et al., 2015; Lentfort et al., 2019).

However, if the clast is foreign, it must have been added to the surface regolith as a xenolith, becoming mixed with other impact-induced CM-clasts of various degrees of aqueous alteration prior to lithification of the Murchison chondrite regolith breccia. This latter process of CM chondrite breccia formation is not clearly indicated in this case, since water-bearing phases are included in the solidification process. Grain-boundary melting during breccia lithification (e.g., Kieffer, 1975; Bischoff et al., 1983, 2006), as found in the case of anhydrous brecciated rocks, has not yet been observed among the CM chondrite breccias.

5. Conclusions

The white clast in Murchison consists of two areas with different granoblastic textures: a coarse-grained and a fine-grained lithology. The Fa-content of olivine in the clast is the same as Fa within olivine from R chondrites; however, the concentrations of Ni and Ca in olivine are significantly different. The O-isotope composition of the clast rules out an R chondrite heritage since it lies in the field of CM chondrites. The occurrence of nepheline-normative glass and maskelynite in a rock with a well-recrystallized texture is very surprising. The white clast may

have formed in the interior of the CM parent body by fluid-assisted percolation during metasomatism triggered by shock-induced annealing.

Acknowledgements

We thank U. Heitmann (Münster), Kent Ross (NASA JSC) for sample preparation and E-Beam assistance, and Kerstin Klemm (Münster), Sarah Lentfort (Münster), and the Heidelberg Ion Probe Team (T. Ludwig, M. Trieloff, and A. Schmitt) for the support during the O-isotope analyses of phases in the xenolithic fragment. We thank Bruno and Carine Fectay for bringing this fascinating sample to our attention and the two anonymous reviewers for their helpful comments and suggestions, as well as the Associate Editor Falko Langenhorst. We also thank the Deutsche Forschungsgemeinschaft (DFG) for support within the SFB-TRR 170″Late Accretion onto Terrestrial Planets" (subproject B05; AB). This is TRR 170 publication No. 64. MEZ was supported by the NASA Emerging Worlds Program.

References

Armstrong, J.T., 1991. Quantitative elemental analysis of individual microparticles with electron beam instruments. In: Heinrich, K.F.J., Newbury, D.E. (Eds.), Electron Probe Quantitation. Plenum Press, New York, pp. 261–315.
Avé-Lallemant, H.G., Carter, N.L., 1970. Syntectonic recrystallization of olivine and modes of flow in the upper mantle. Geol. Soc. Am. Bull. 81 (2003), 2020.
Barrat, J.-A., Zanda, B., Moynier, F., Bollinger, C., Liorzou, C., Bayron, G., 2012. Geochemistry of CI chondrites: major and trace elements, and Cu and Zn isotopes. Geochim. Cosmochim. Acta 83, 79–92.
Berlin, J., Stöffler, D., 2004. Modification of the van schmus & Wood petrologic classification for lithic fragments in the chondritic breccia rumuruti. 35th Lunar Planetary Science Conference. Houston(abstract #1344).
Beyer, E., Griffin, W.L., O'Reilly, S.Y., 2006. Transformation of Archaean lithospheric mantle by refertilization: evidence from exposed peridotites in the Western Gneiss Region, Norway. J. Petrol. 47, 1611–1636.
Bischoff, A., 1998. Aqueous alteration of carbonaceous chondrites: evidence for preaccretionary alteration - a review. Meteoritics Planet. Sci. 33, 1113–1122.
Bischoff, A., Schultz, L., 2004. Abundance and meaning of regolith breccias among meteorites. Meteoritics Planet. Sci. 39, A15.
Bischoff, A., Stöffler, D., 1992. Shock metamorphism as a fundamental process in the evolution of planetary bodies: information from meteorites. Europ. J. Mineral 4, 707–755.
Bischoff, A., Rubin, A.E., Keil, K., Stöffler, D., 1983. Lithification of gas-rich chondrite regolith breccias by grain boundary and localized shock melting. Earth Planet. Sci. Lett. 66, 1–10.
Bischoff, A., Scott, E.R.D., Metzler, K., Goodrich, C.A., 2006. Nature and origins of meteoritic breccias. In: Lauretta, D.S., McSween Jr.H.Y. (Eds.), Meteorites and the Early Solar System II. University of Arizona Press, pp. 679–712.
Bischoff, A., Vogel, N., Roszjar, J., 2011. The Rumuruti chondrite group – invited review. Chemie Der Erde - Geochem. 71, 101–134.
Bischoff, A., Ebert, S., Metzler, K., Lentfort, S., 2017. Breccia classification of CM chondrites (abstract #6089). Meteorit. Planet. Sci. 52, A26 #6089.
Bischoff, A., Patzek, M., Ebert, S., Pack, A., Kerraouch, I., Zolensky, M.E., 2018. A large, light fragment in the Murchison (CM) breccia - a unique, highly-metamorphosed chondrite as a xenolith in a CM chondrite (abstract #6217). Meteorit. Planet. Sci. 53, 6217.
Brearley, A.J., Lauretta, D.S., McSween Jr, H.Y., 2006. The action of water. Meteorites and the Early Solar System II. University of Arizona Press, pp. 587–624.
Brearley, A.J., Jones, R.H., 1998. Chondritic meteorites. In: Papike, J.J. (Ed.), Planetary Materials. Mineralogical Society of America, Washington, D. C pp. 3-1-3-398.
Clayton, R.N., Mayeda, T.K., 1999. Oxygen isotope studies of carbonaceous chondrites. Geochim. Cosmochim. Acta 63, 2089–2104.
Costa, F., Chakraborty, S., 2008. The effect of water on Si and O diffusion rates in olivine and implications for transport properties and processes in the upper mantle. Phys. Earth Planet. Inter. 166, 11–29.
Demouchy, S., Mackwell, S.J., Kohlstedt, D.L., 2007. Influence of hydrogen on Fe–Mg interdiffusion in (Mg,Fe)O and implications for Earth's lower mantle. Contrib. Mineral. Petrol. 154, 279–289.
Dodd, R.T., 1969. Metamorphism of the ordinary chondrites: a review. Geochim. Cosmochim. Acta 33, 161–203.
Ebert, S., Patzek, M., Bischoff, A., 2018. Xenolithic fragment in the CM chondrite Mukundpura: greetings from the Tucson parent body? (abstract #6246). Meteorit. Planet. Sci. 53, 6246.
Ebert, S., Bischoff, A., Harries, D., Lentfort, S., Barrat, J.-A., Pack, A., Gattacceca, J., Visser, R., Schmid-Beurmann, P., Kimpel, S., 2019. Northwest Africa 11024 – a heated and dehydrated unique carbonaceous (CM) chondrite. Meteorit. Planet. Sci. 54, 328–356.
Fodor, R., Keil, K., 1976. Carbonaceous and noncarbonaceous lithic fragments in the Plainview, Texas chondrite: origin and history. Geochim. Cosmochim. Acta 40, 177–189.
Fodor, R.V., Keil, K., Wilkening, L.L., Bogard, D.D., Gibson, E.K., 1976. Origin and history of a meteorite parent-body regolith breccia: carbonaceous lithic fragments in the Abbott, New Mexico, chondrite. Special Pub. New Mexico Geol. Soc. 6, 206–218.
Gardner-Vandy, K.G., Lauretta, D.S., McCoy, T.J., 2013. A petrologic, thermodynamic and experimental study of brachinites: partial melt residues of an R chondrite-like precursor. Geochim. Cosmochim. Acta 122, 36–57.
Greenwood, J.P., Rubin, A.E., Wasson, J.T., 2000. Oxygen isotopes in R chondrite magnetite and olivine: links between R chondrites and ordinary chondrites. Geochim. Cosmochim. Acta 64, 3897–3911.
Greenwood, R.C., Franchi, I.A., Gibson, J.M., Benedix, G.K., 2012. Oxygen isotopic variation in primitive achondrites: the influence of primordial, asteroidal and terrestrial processes. Geochim. Cosmochim. Acta 94, 146–163.
Hertkorn, N., Harir, M., Schmitt-Kopplin, Ph., 2015. Nontarget analysis of Murchison soluble organic matter by high-field NMR spectroscopy and FTICR mass spectrometry. Magn. Reson. Chem. 53, 754–768.
Hewins, R.H., Bourot-Denise, M., Zanda, B., Leroux, H., Barrat, J.-A., Humayun, M., Göpel, C., Greenwood, R.C., Franchi, I.A., Pont, S., Lorand, J.-P., Cournede, C., Gattacceca, J., Rochette, P., Kuga, M., Marrocchi, Y., Marty, B., 2014. The Paris meteorite, the least altered CM chondrite so far. Geochim. Cosmochim. Acta 124, 190–222.
Hier-Majumder, S., Anderson, I.M., Kohlstedt, D.L., 2004. Influence of Protons on Fe-Mg interdiffusion in olivine. J. Geophys. Res. B2, B02202.
Imae, N., Zolensky, M.E., 2003. Mineralogy and petrology of a rumuruti chondrite, including a large unequilibrated clast: PRE95404. International Symposium—Evolution of Solar System Materials: A New Perspective from Antarctic Meteorites.
Isa, J., Rubin, A.E., Wasson, J.T., 2014. R chondrite bulk-chemical compositions and diverse oxides: implications for parent-body processes. Geochim. Cosmochim. Acta 124, 131–151.
Jung, H., Karato, S.I., 2001b. Effects of water on dynamically recrystallized grain-size of olivine. J. Struct. Geol. 23 (9), 1337–1344.
Jochum, Klaus Peter, et al., 2005. GeoReM: a new geochemical database for reference materials and isotopic standards. Geostandards Res. Geoanal Vol 29-N3.
Karato, S., 1989. Grain growth kinetics in olivine aggregates. Tectonophysics 168, 255–273.
Karato, S., Rubie, D.C., Yan, H., 1993. Dislocation recovery in olivine under deep upper mantle conditions-Implications for creep and diffusion. J. Geophys. Res. 20 (5), 315–322.
Kerraouch, I., Zolensky, M.E., Bischoff, A., Le, L., Belhaï, D., Patzek, M., Ebert, S., 2018. Mineralogical study of a white clast from Murchison (CM2): comparison with R chondrites (abstract #6363). Meteorit. Planet. Sci. 53, 6363.
Kieffer, S.W., 1975. From regolith to rock by shock. Moon 13, 301–320.
Lee, C.-T.A., 2003. Compositional variation of density and seismic velocities in natural peridotites at STP conditions: implications for seismic imaging of compositional heterogeneities in the upper mantle. J. Geophys. Res. 108 (B9), 2441.
Lenoir, X., Garrido, C., Bodinier, J.-L., Dautria, J.-M., Gervilla, F., 2001. The recrystallization front of the Ronda peridotite: evidence for melting and thermal erosion of subcontinental lithospheric mantle beneath the Alboran Basin. J. Petrol. 42, 141–158.
Lentfort, S., Bischoff, A., Ebert, S., 2019. Classification of 13 CM chondrite breccias and CM clasts in two achondrites (abstract #6029). Meteorit. Planet. Sci. 54 #6029.
Le Roux, V., Bodinier, J.-L., Tommasi, A., Alard, O., Dautria, J.-M., Vauchez, A., Riches, A.J.V., 2007. The Lherz spinel lherzolite: refertilized rather than pristine mantle. Earth Planet. Sci. Lett. 259, 599–612.
Le Roux, V., Tommasi, A., Vauchez, A., 2008. Feedback between melt percolation and deformation in an exhumed lithosphere–asthenosphere boundary. Earth Planet. Sci. Lett. 274, 401–413.
Lindgren, P., Lee, M.R., Sofe, M.R., Zolensky, M.E., 2013. Clasts in the CM2 carbonaceous chondrite Lonewolf Nunataks 94101:evidence for aqueous alteration prior to complex mixing. Meteorit. Planet. Sci. 48, 1074–1090.
Lodders, K., Fegley Jr, B., 1998. The Planetary Scientist`s Companion. Oxford University Press, New York 371 pp.
Metzler, K., Bischoff, A., Stoffler, D., 1992. Accretionary dust mantles in CM chondrites: Evidence for solar nebula processes. Geochim. Cosmochim. Acta 56, 2873–2898.
Metzler, K., Bischoff, A., 1996. Constraints on chondrite agglomeration from fine-grained chondrule rims. In: Hewins, R.H., Jones, R.H., Scott, E.R.D. (Eds.), Book Chapter in: "Chondrules and the Protoplanetary Disk". Cambridge University Press, pp. 153–162.
Mittlefehldt, D.W., 2006. Achondrites. In meteorites, comets, and planets, edited by. In: In: Davis, A.M. (Ed.), Treatise on Geochemistry, Oxford, vol. 1. Elsevier Science, Amsterdam, pp. 291–324.
Müntener, O., Pettke, T., Desmurs, L., Meier, M., Schaltegger, U., 2004. Refertilization of mantle peridotite in embryonic ocean basins: trace element and Nd isotopic evidence and implications for crust–mantle relationships. Earth Planet. Sci. Lett. 221, 293–308.
Pack, A., Tanaka, R., Hering, M., Sengupta, S., Peters, S., Nakamura, E., 2016. The oxygen isotope composition of San Carlos olivine on VSMOW2-SLAP2 scale, Rapid Commun. Mass Spectrom. 30, 1495–1504.
Patzek, M., Bischoff, A., Visser, R., John, T., 2018. Mineralogy of volatile-rich clasts in brecciated meteorites. Meteorit. Planet. Sci. 53, 2519–2540.
Rampone, E., Piccardo, G.B., Vannucci, R., Bottazzi, P., Zanetti, A., 1994. Melt impregnation in ophiolitic peridotite: an ion microprobe study of clinopyroxene and plagioclase. Mineral. Mag. 58A, 756–757.
Rubin, A.E., Kallemeyn, G.W., 1994. Pecora Escarpment 91002: a member of the new Rumuruti (R) chondrite group. Meteoritics 29, 255–264.
Rubin, A.E., Trigo-Rodríguez, J.M., Huber, H., Wasson, J.T., 2007. Progressive aqueous alteration of CM carbonaceous chondrites. Geochim. Cosmochim. Acta 71, 2361–2382.

Rubin, A.E., Wasson, J., 1986. Chondrules in the Murray CM2 meteorite and compositional differences between CM-CO and ordinary chondrite chondrules. Geochim. Cosmochim. Acta 50, 307–315.

Ruf, A., Kanawati, B., Hertkorn, N., Yin, Q.Z., Moritz, F., Harir, M., Lucio, M., Michalke, B., Wimpenny, J., Shilobreeva, S., Bronsky, B., Saraykin, V., Gabelica, Z., Gougeon, R., Quirico, E., Ralew, S., Jakubowski, T., Haack, H., Jenniskens, P., Hinman, N.W., Schmitt-Kopplin, Ph., 2017. Previously unknown class of metalorganic compounds revealed in meteorites. Proc. Natl. Acad. Sci. https://doi.org/10.1073/pnas.1616019114.

Schmitt-Kopplin, Ph., Gabelica, Z., Gougeon, R.D., Fekete, A., Kanawati, B., Harir, M., Gebefuegi, I., Eckel, G., Hertkorn, N., 2010. High molecular diversity of extraterrestrial organic matter in Murchison meteorite revealed 40 years after its fall. PNAS 107 (7), 2763–2768.

Schmitt-Kopplin, Ph., Harir, M., Kanawati, B., Tziotis, D., Hertkorn, N., Gabelica, Z., 2012. Chemical footprint of the solvent soluble extraterrestrial organic matter occluded in Sołtmany ordinary chondrite. Meteorite Journal, Special issue *Soltmany* 1–2, 79–92.

Schulze, H., Bischoff, A., Palme, H., Spettel, B., Dreibus, G., Otto, J., 1994. Mineralogy and chemistry of Rumuruti: the first meteorite fall of the new R chondrite group. Meteoritics 29, 275–286.

Sharp, Z.D., 1990. A laser-based microanalytical technique for in situ determination of oxygen isotope ratios of silicates and oxides. Geochim. Cosmochim. Acta 54, 1353–1357.

Soustelle, V., Tommasi, A., Bodinier, J.-L., Garrido, C.J., Vauchez, A., 2009. Deformation and reactive melt transport in the mantle lithosphere above a large-scale partial melting domain: the Ronda peridotite massif, S Spain. J. Petrol. 50 (7), 1235–1266.

Stöffler, D., Keil, D., Scott, E.R.D., 1991. Shock metamorphism of ordinary chondrites. Geochim. Cosmochim. Acta 55, 3845–3867.

Takenouchi, A., Zolensky, M., Nishiizumi, K., Caffee, M., Velbel, M., Ross, K., Zolensky, A., Le, L., Imae, N., Yamaguchi, A., Mikouchi, T., 2013. What are space exposure histories telling us about CM carbonaceous chondrites. 2013 NIPR Symposium on Antarctic Meteorites.

Tommasi, A., Godard, M., Coromina, G., Dautria, J.-M., Barsczus, H., 2004. Seismic anisotropy and compositionally induced velocity anomalies in the lithosphere above mantle plumes: a petrological and microstructural study of mantle xenoliths from French Polynesia. Earth Planet. Sci. Lett. 227, 539–556.

Tommasi, A., Vauchez, A., Godard, M., Belley, F., 2006. Deformation and melt transport in a highly depleted peridotite massif from the Canadian Cordillera: implications to seismic anisotropy above subduction zones. Earth Planet. Sci. Lett. 252, 245–259.

Tommasi, A., Vauchez, A., Ionov, D., 2008. Deformation, static recrystallization, and reactive melt transport in shallow subcontinental mantle xenoliths (Tok Cenozoic volcanic field, SE Siberia). Earth Planet. Sci. Lett. https://doi.org/10.1016/j.epsl.2008.1004.1020.

Tonui, E., Zolensky, M., Hiroi, T., Nakamura, T., Lipschutz, M., Wang, M.-S., Okudaira, K., 2014. Petrographic, chemical and spectroscopic evidence for thermal metamorphism in carbonaceous chondrites I: CI and CM chondrites. Geochim. Cosmochim. Acta 126, 284–306.

Tziotis, D., Hertkorn, N., Schmitt-Kopplin, Ph., 2011. Kendrick-analogous network visualisation of ion cyclotron resonance fourier transform (FTICR) mass spectra: improved options to assign elemental compositions and to classify organic molecular complexity. Eur. J. Mass Spectrom. 17, 415–421.

Van Schmus, W.R., Wood, J.A., 1967. A chemical- petrologic classification for the chondritic meteorites. Geochim. Cosmochim. Acta 31 747–747.

Vauchez, A., Garrido, C.J., 2001. Seismic properties of an asthenospherized lithospheric mantle: constraints from lattice preferred orientations in peridotite from the Ronda massif. Earth Planet. Sci. Lett. 192 (2), 235–249.

Verdier-Paoletti, M.J., Marrocchi, Y., Avice, G., Roskosz, M., Gurenko, A., Gounelle, M., 2017. Oxygen isotope constraints on the alteration temperatures of CM chondrites. Earth Planet. Sci. Lett. 458, 273–281.

Zolensky, M.E., Hewins, R.H., Mittlefehldt, D.W., Lindstrom, M.M., Xiao, X., Lipschutz, M.E., 1992. Mineralogy, petrology and geochemistry of carbonaceous chondritic clasts in the LEW 85300 polymict eucrite. Meteoritics 27, 596–604.

Zolensky, M.E., Weisberg, M.K., Buchanan, P.C., Mittlefehldt, D.W., 1996. Mineralogy of carbonaceous chondrite clasts in HED achondrites and the Moon. Meteorit. Planet. Sci. 31, 518–537.

Zolensky, M.E., Gregory, T., Takenouchi, A., Nishiizumi, K., Trieman, A., Berger, E., Le, L., Fagan, A., Velbel, M., Imae, N., Yamaguchi, A., Caffee, M., 2015. CM carbonaceous chondrite lithologies and their space exposure ages. 2015 NIPR Symposium on Antarctic Meteorites.